

# GCM SIMULATIONS OF TRANSIENT EDDIES AND FRONTAL SYSTEMS IN THE MARTIAN ATMOSPHERE

**R. J. Wilson**, *Geophysical Fluid Dynamics Laboratory, Princeton, NJ (John.Wilson@noaa.gov)*, **D. Hinson**, *Stanford University, Stanford, CA* and **M. D. Smith**, *NASA Goddard Space Flight Center, Greenbelt, MD., USA*.

**Introduction:** The outstanding problem for simulating the present Mars climate is representing the spatial and temporal variability of aerosol and the feedbacks that connect dust raising and transport with the evolving atmospheric circulation. Over 3 Mars years of observations by Mars Global Surveyor has provided an emerging climatology of dust activity. Figure 1 summarizes the season variation of zonally-averaged dust opacity. Apart from the global dust storm of Mars Year 25 (MY25), there is a clear pattern of prominent dust storm activity in two seasonal windows before and after northern winter solstice ( $L_s = 200\text{-}240^\circ$  and  $L_s = 305\text{-}340^\circ$ ). This activity is also reflected in global mean temperatures [Smith, 2004]. The initiation and evolution of a number of regional scale dust storms has been documented in detail with MOC imagery and TES temperature and dust opacity observations [Cantor *et al.*, 2001; Wang *et al.*, 2005]. These storms are evidently associated with traveling waves embedded in the strong westerly jet that is present in the northern hemisphere in the fall, winter and spring seasons. Dust raising activity initiated by these transient wave events propagates southward towards (and across) the equator in north-south oriented channels defined by the low topography regions: Acidalia into Chryse, Arcadia into Amazonis and Utopia into Isidis [Wang *et al.* 2003, 2005]. This regional storm behavior has been referred to as a “flushing” storm [Wang *et al.* 2003]. Upon reaching low latitudes, they can rapidly intensify and spread, often yielding the highest dust optical depths at low to mid southern latitudes. Such storm event sequences account for the 5 opacity peaks evident in Fig. 1. Thus it appears that these “flushing” storms significantly contribute to the seasonal cycle of dust and global mean temperature.

The evident association of traveling waves with a prominent aspect of the Mars dust cycle motivates our investigation of the characteristics and climatology of transient waves in the GFDL Mars general circulation model (MGCM). We also consider high-resolution simulations with interactive dust lifting that provide insight into the storm intensification stage as dust is transported southward through the flushing channels into the southern hemisphere (SH).

**General Circulation Model:** The GFDL MGCM simulates the circulation of the Martian atmosphere with a comprehensive set of physical parameterizations

[Wilson and Hamilton, 1996]. These include parameterizations for radiative transfer associated with  $\text{CO}_2$  gas and aerosols. The aerosol fields may be specified or can be allowed to evolve with the circulation following prescribed or interactive lifting at the surface. Simulations with interactive dust lifting are described in Basu *et al.* [2004] and Basu *et al.* (this workshop). The inclusion of predicted water ice clouds provides an additional means of comparing the simulated circulations with observed ice cloud morphologies. The predicted ice clouds are optionally radiatively active [Hinson and Wilson, 2004]. We find that radiatively active polar hood clouds can influence the thermal structure of the polar vortex, particularly in the equinoctial seasons, thus affecting the simulated transient wave response. Simulations have been carried out at  $5^\circ \times 6^\circ$ ,  $3^\circ \times 5^\circ$  and  $2^\circ \times 2.4^\circ$  resolutions.

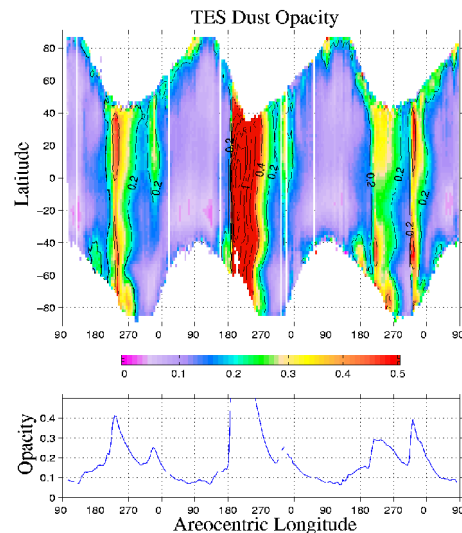


**Figure 1.** (a) The seasonal variation of dust column opacity observed by TES for 3 Mars years (MY24 into MY27). (b) The variation of tropical opacity. The 2001 global dust storm occurs at  $L_s = 187$  in MY25. The other 5 opacity peaks are associated with “flushing” storm events.

**Surface Stresses:** Characterizing the spatial and temporal patterns of surface stress is an important step for assessing the potential for MGCM simulation of the Mars dust cycle. Figure 2 shows the seasonal evolution of zonally averaged surface stress from a simulation with relatively weak dust loading. This stress pattern

is, however, representative of results from GCM simulations covering a range of dust loading scenarios. We can identify different circulation elements with the various regions of notable stress. Note that significantly larger values are obtained in specific locations and local times, as suggested by Figure 3, which shows the spatial distribution of the average maximum stress for each model grid box in a 10 year simulation. The variance of this average maximum is one measure of interannual variability. In regions where the maximum surface stress is dominated by tides, there will be little interannual variability (in any given simulation with fixed dust). For example, tides dominate variability in the Hellas region during the peak of SH summer season while traveling waves (with interannual variability) are an important component of the stress history in the SW corner of Hellas in the  $L_s = 170\text{-}200^\circ$  season.

One region of strong surface stresses in Fig. 2 is in the SH subtropics during southern summer. These winds are associated with the shallow subtropical jet that forms in response to Coriolis deflection of the strong cross-equatorial winds that comprise the lower branch of the Hadley circulation in this season. These stresses are modulated by topography and have a strong local time dependence. The strength of the subtropical jet varies with dust optical depth.

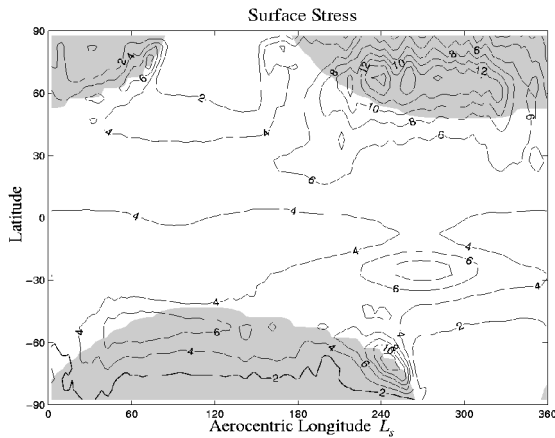


**Figure 2** Simulated seasonal variation of zonally and diurnally averaged surface stress. Units are  $10^{-3} \text{ Nm}^{-2}$ . Shading indicates the variable extent of the  $\text{CO}_2$  ice caps.

Another band of high surface stress occurs along the edges of the retreating  $\text{CO}_2$  ice caps during the spring season in each hemisphere. The strong thermal contrast between the ice-free and cap surface results in an intense local circulation with a marked diurnal variation. Spacecraft observations indicate frequent local scale dust activity in these regions so that it appears that this activity is a ubiquitous feature of the current Mars climate. These stresses are sensitive to the inclu-

sion of radiatively active water ice clouds, which can have a strong influence on polar vortex in the spring seasons. Shallow, traveling waves are simulated along the  $\text{CO}_2$  ice cap boundary. In the SH, this stress is particularly localized to the Hellas and Argyre basins during the  $L_s = 150\text{-}200^\circ$  season and becomes more zonally uniform later in the season. These waves are likely of significance for dust storm activity in the Hellas region in the  $L_s = 60$  and  $180^\circ$  seasons. There is evidence in MOC imagery [Strausberg *et al.* 2005] and TES thermal retrievals that eastward traveling waves played an important role in the initiation of the 2001 global storm that began in the Hellas basin.

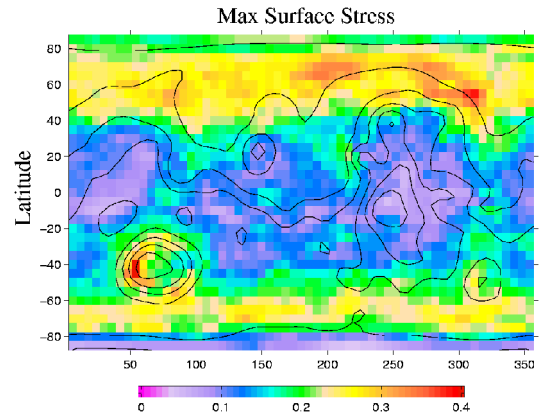


**Figure 3.** Spatial distribution of average maximum surface stress within an annual cycle. Units are  $10^{-1} \text{ Nm}^{-2}$ . Model topography ( $5^\circ \times 6^\circ$ ) resolution is contoured.

The strong stresses evident in the NH during the fall, winter and spring ( $L_s = 180\text{-}350^\circ$ ) season are associated with the westerly jet that forms in this season. Traveling waves account for much of the strength and variability of stress in this region. Increasing dust loading leads to a weakening of the stresses associated with the midlatitude westerlies. Significantly, the surface stresses diminish sharply during the NH winter solstice season when the dust loading is increased. This is due to the suppression of baroclinic wave activity. The intensification of the Hadley circulation under high obliquity conditions has the same effect. This decline in transient wave activity at solstice was noted at the Viking lander 2 site following the 1977b global dust storm and is evident in the other GCM simulations.

**Transient Wave Analysis:** MGCM model output has been archived and selected fields have been band-pass filtered to eliminate thermal tides and quasi-stationary waves. This allows us to focus on transient wave activity, here defined as wave with periods from 1.5 to 10 sols. Figure 4 shows a representative seasonal variation of the zonally averaged eddy compo-

ment of the meridional velocity. A clear pattern of pre and post solstice activity is evident, with peak periods of wave activity at  $L_s=190-240^\circ$  and  $L_s=310-350^\circ$  and relatively little activity at solstice. This pattern of reduced eddy activity at solstice is enhanced as the dust loading is increased and is consistent with the expectation of increased stabilization of shorter waves with increasing atmospheric static stability. This simulation employs a generally larger dust column than the simulation shown in Fig. 2. The seasonal variation in eddy activity in Fig. 4 corresponds closely to the periods of flushing storm activity responsible for the observed opacity peaks in Fig. 1. There is a notable peak in wave activity in the SH from  $L_s = 180$  to  $230^\circ$ .

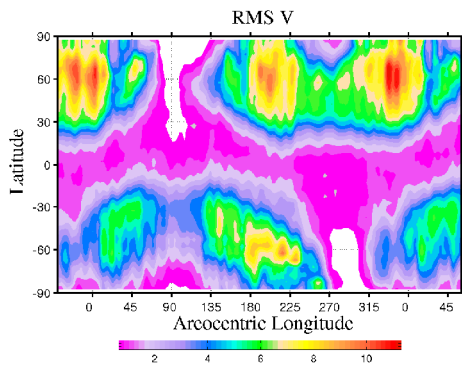


**Figure 4.** Seasonal evolution of the zonally-averaged eddy V variance (bandpass filtered 1.5-10 sols) from a simulation employing MGS opacities. Units are  $\text{ms}^{-1}$ .

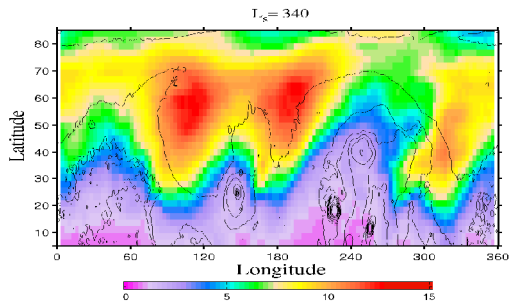


**Figure 5.** Spatial distribution of the rms V field for late NH winter. Amplitude in  $\text{ms}^{-1}$

Figure 5 shows the spatial distribution of the rms amplitude of the near-surface meridional wind. Similar presentations can be made with temperature, which can be directly compared with TES observations [Banfield et al. 2004; Wang et al. 2005]. The strongest mid-latitude eddy activity occurs in the 3 low-level channels (Acidalia, Arcadia and Utopia) that are observed to be active locations of flushing wave events [Wang et al. 2003, 2005] and which have been regarded as a storm track structure [Hollingsworth et al. 1996].

The filtered fields have also been passed through a space-time spectral analysis. Transient wave activity is found to be dominated by eastward propagating waves with zonal wavenumbers 1 through 3. The low-level eddy wind fields are dominated by zonal wave 3, while other fields reflect a seasonally-varying mix of waves 1 through 3. The simulated waves have periods of  $\sim 7$  sols, 3-4 sols and  $\sim 2$  sols for wavenumbers 1 through 3, respectively. This is in very good agreement with observations [e.g. Banfield et al. 2004]. An analysis of the vertical structure of the eddy fields shows increasing vertical confinement of wave amplitude with increasing wavenumber. Transitions in dominant wavenumber are evident in both observations [Banfield et al. 2004] and in simulations [Barnes et al. 1993; Collins et al. 1996].

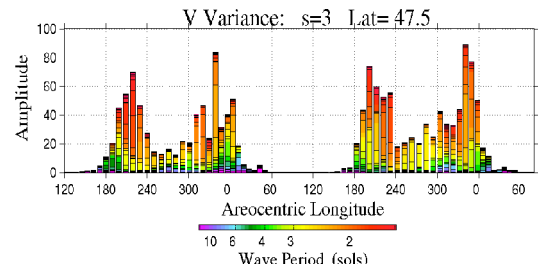


**Figure 6.** Histogram showing the seasonal variation of the eastward propagating, zonal wave 3 component of the meridional velocity (at 1 km). Units in  $\text{m}^2\text{s}^{-2}$ . The color coding indicates that waves with periods of  $\sim 2$  sols make the dominant contribution to the variance.

The dominant spatial structures of the traveling waves may be represented using a principal components (PC) analysis. Typically, a small subset of PCs is sufficient to explain the bulk of transient wave variance. The dominant PCs (sorted by explained variance) tend to appear in pairs and an examination of the time series of the projection of the data onto these PCs confirms the eastward propagating character. The top 3 pairs of PCs have patterns with zonal wave 1, 2 and 3 character.

The seasonal variation of the eastward propagating zonal wave 3 component of meridional velocity is shown in Figure 6. The color coding indicates that waves with periods of  $\sim 2$  sols make the dominant contribution to the variance at this wavelength.

A representative snapshot of eddy field structure ( $L_s=336^\circ$ ) is shown in Fig 7. A wave 3 character is clearly evident in the eddy temperature, pressure and velocity fields. These fields coherently propagate eastward with a  $\sim 2$  sol period. There is strong southward advection in the cold regions and northward motion in the warm sectors consistent with classical frontal structure associated with low pressure systems. As suggested

in figure 5, there is greater southward penetration of the fronts in the 3 lowland channels, as confirmed by examination of animations.

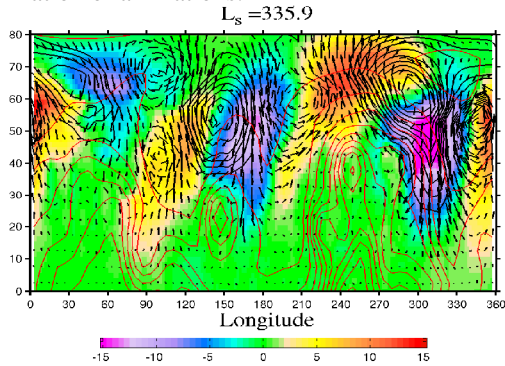


**Figure 7.** Spatial variation of eddy fields at 2 km. The eddy temperature field is shaded while the eddy pressure fields are plotted with dotted (negative) and solid (positive) black contours. The eddy wind field is shown by the arrows. Model topography is indicated by red contours

**Interactive dust lifting:** We have carried out simulations of dust storm initiation and development with simple dust lifting parameterizations based on surface stress. Some of these are presented in *Basu et al.* (this workshop). Similar work is described by *Newman et al.* [2002]. Figure 8 shows a flushing storm event in the Chryse basin from a high-resolution ( $2^\circ \times 2.4^\circ$ ) simulation run from  $L_s = 210$  to  $260^\circ$ . The eddy fields have a prominent 2-sol period for much of the time interval. A sequence of several flushing events were obtained in the  $L_s = 225$  to  $232^\circ$  period, resulting in peak atmospheric opacity at  $L_s \sim 235^\circ$ . The dust front has reached  $25^\circ$  N in the figure and is in the process of augmenting dust from the previous flushing event. The surface stresses are sufficiently high in the dust band that additional lifting is taking place. At this latitude, the tide circulation makes a significant contribution to surface stress. The eddy fields were appropriately synchronized with the thermal tide to result in efficient southward transport of dust into the tropics, as proposed by *Wang et al.* [2003]. The  $\sim 2$  sol period constitutes a subharmonic resonance with the diurnal tide. The tide circulation in the Chryse basin has the character of an afternoon upslope wind [*Wilson and Hamilton* 1996] that is in phase with the global scale thermal tide. This contributes to a positive feedback between dust loading and tide amplitude.

This sort of simulation will be useful for developing improved representations for dust lifting and assessing the interplay between circulation elements and radiative feedbacks that likely accounts for Martian dust storm activity.

## References:

- Banfield, D., B.J. Conrath, M.D. Smith, P.R. Christensen, and R.J. Wilson, Forced waves in the Martian atmosphere from MGS TES nadir data, *Icarus*, *161*, 319-345, 2003.
- Barnes J.R., et al., Mars atmospheric dynamics as simulated by the NASA Ames general circulation model.2. transient baroclinic eddies, *J. Geophys. Res.*, *98*, 3125-3148, 1993.
- Basu, S., M.I. Richardson, and R.J. Wilson, Simulation of the martian dust cycle with the GFDL Mars GCM, *J. Geophys. Res.*, *109*, E11906, 2004.
- Cantor, B.A., P.B. James, M. Caplinger, and M.J. Wolff, Martian dust storms: 1999 Mars Orbiter Camera observations, *J. Geophys. Res.*, *106*(E10), 23653-23687, 2001.
- Collins, M., et al., Baroclinic wave transitions in the Martian atmosphere, *Icarus*, *120*, 344-357, 1996.
- Hinson, D., and R.J. Wilson, Temperature inversions, thermal tides, and water ice clouds in the Martian tropics, *J. Geophys. Res.*, *109*, E01002, 2004.
- Hollingsworth, J. L., et al., Orographic control of storm zones on Mars, *Nature*, *380*, 413-416, 1996.
- Newman, C.E., et al., Modeling the dust cycle in a Mars general circulation model, 2: Multiannual radiatively active dust transport simulations, *J. Geophys. Res.*, *107*(E12), 2002
- Smith, M.D., Interannual variability in TES Atmospheric observations of Mars during 1999-2003, *Icarus*, *108*, 148-165, 2004.
- Wang, H., M.I. Richardson, R.J. Wilson, A.P. Ingersoll, and R.W. Zurek (2003), Cyclones, tides, and the origin of major dust storms on Mars, *Geophys. Res. Lett.*, 2003.
- Wang, H., R.W. Zurek, and M.I. Richardson, The relationship between frontal dust storms and transient eddy activity in the northern hemisphere of Mars as observed by Mars Global Surveyor, *J. Geophys. Res.*, *110*, 2005.
- Wilson, R.J., and K.P. Hamilton, Comprehensive model simulation of thermal tides in the martian atmosphere, *J. Atmos. Sci.* *53*, 1290-1326, 1996.
- Wilson, R.J., D. Banfield, B.J. Conrath, and M.D. Smith, Traveling waves in the northern hemisphere of Mars, *Geophys. Res. Lett.*, *29*(14), 10.1029/2002GL014866, 2002.

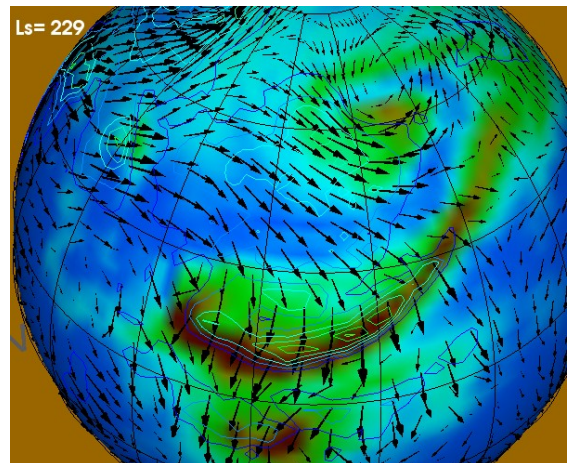


**Figure 8.** High resolution simulation of a frontal system in the Chryse basin showing column dust opacity (shaded) and low-level ( $\sim 1$  km) winds. High values of surface stress are indicated by contour lines. The figure is centered on  $330^\circ$  E,  $40^\circ$  N. The signature of the eddy low pressure center is evident in the "rolling up" of the dust filament at  $60^\circ$  N.